Available online at www.sciencedirect.com
ScienceDirect
Journal of Computational Physics 225 (2007) 6–12
JOURNAL OF COMPUTATIONAL PHYSICS
www.elsevier.com/locate/jcp

Short Note

Nonmonotone chemotactic invasion: High-resolution simulations, phase plane analysis and new benchmark problems

Matthew J. Simpson *, Kerry A. Landman

Department of Mathematics and Statistics, University of Melbourne, Victoria 3010, Australia

Received 7 December 2006; received in revised form 20 March 2007; accepted 22 March 2007
Available online 31 March 2007

Keywords: Hyperbolic conservation law; Chemotaxis; Invasion; High-resolution methods; Shocks

1. Introduction

Verifying and validating the performance of a computational simulation is a challenging problem of interest in all applied sciences [12,13]. Measuring the performance of a numerical algorithm against standard benchmark test cases is often the first step in assessing algorithm performance. These test cases are used repeatedly over long periods of time as algorithms are devised and improved. In addition, new benchmark test cases are continually developed [9]. Effective benchmarks are characterized by having either a complete or an approximate analytical solution against which the numerical results can be quantitatively compared [1,5]. It is also possible, although less common, to use carefully collected laboratory data to benchmark a numerical code [18,22].

To identify an effective benchmark test case, a balance must be found between two opposing requirements: the benchmark ought to be sufficiently complex to rigorously challenge a numerical algorithm, and it should also be amenable to analysis.

Certain problems have become synonymous with algorithm development in various disciplines. Particular problems from fluid mechanics, for example, are associated with long-celebrated benchmarks. Algorithms designed to solve steady incompressible Navier–Stokes flows are often tested with lid-driven cavity flow problems and Burggraf's solution [1,3]. Algorithms designed to solve convectively-driven flow in porous media are usually benchmarked with Henry's solution for salt water intrusion [5,19]. Many other examples of popular benchmark test cases can be found in the literature.

Constructing numerical algorithms to accurately approximate the solution of hyperbolic conservation laws (HCL) is of wide interest and challenging. Typically HCL algorithms are tested with a suite of benchmark problems starting with single species linear advection [2,3,6,10]. Linear advection has the advantage of being conceptually simple, analytically tractable and clearly identifies susceptibility to numerical diffusion and

* Corresponding author. Tel.: +61 3 83446517; fax: +61 3 83444599.
E-mail address: m.simpson@ms.unimelb.edu.au (M.J. Simpson).

0021-9991/$ - see front matter
doi:10.1016/j.jcp.2007.03.016

artificial oscillation. Beyond single species linear advection, algorithms are often benchmarked with Burger's equation. This problem retains the simplicity of a single species HCL with the complexity of introducing a nonlinear flux which tests an algorithm's ability to predict shock formation. Perhaps the most common benchmark for HCL algorithms is Sod's shock tube problem [21]. This is a rigorous benchmark requiring the solution of three coupled nonlinear equations. Sod's shock tube problem is used to test whether a code can predict solutions with multiple discontinuities. Variants of Sod's problem have been used for code development in numerous applications including dam break phenomena [23], star formation [17] and the dynamics of volcanic ash plumes [14].

Although various other HCL benchmarks are used for algorithm development, such as traffic flow problems, acoustic dynamics and the Buckley–Leverett equation [2,3,6,10], there does not appear to be any particular problem more complex than the shock tube problem that has become a clear standard choice for benchmarking. We propose a new test case which has arisen in computational biology relevant to chemotactic cell invasion [15,20]. The invasion problem involves nonlinearities and coupling in both the flux and source terms. These features make the numerical solution of the invasion problem more challenging than the shock tube problem. However, at the same time, many properties of traveling wave solutions to the invasion problem can be deduced exactly with nonstandard phase plane analysis. The invasion problem is sufficiently rigorous that it tests an algorithm's ability to approximate solutions with multiple discontinuities and complicated nonmonotone profiles.

A major historical difficulty in developing numerical algorithms for HCLs is the formation of artificial numerical oscillations. These oscillations often appear close behind a shock [10,21]. In this work we present an unusual test case where the true analytical solution is nonmonotone with an oscillatory region appearing just behind a shock. Therefore the correct solution has certain properties which are not shared by standard benchmark test cases.

We will briefly present the invasion model, describe the analysis, specify certain test cases and quantitatively compare numerical and analytical results. The details of a suite of solutions are tabulated for benchmarking purposes.

2. Chemotactic invasion model

Conservation of mass for chemotactic migration of cells with density n and chemoattractant concentration g in one spatial dimension gives

$$\frac{\partial n}{\partial t} = -\frac{\partial}{\partial x}\left(\chi(g) n \frac{\partial g}{\partial x}\right) + f(n), \quad \frac{\partial g}{\partial t} = h(g,n). \tag{1}$$

Here x is the spatial coordinate, t is time and $\chi(g)$ is the chemotactic sensitivity function. In these scaled equations we specify the source term for n as a logistic proliferation term $f(n) = n(1-n)$. The source term for g incorporates zeroth order production, linear decay and a nonlinear uptake term as given by $h(g,n) = \beta(1-g) - \gamma n g$. This system is strictly hyperbolic and details of the scaling used to nondimensionalize Eq. (1) are given elsewhere [20].

Most applications of hyperbolic invasion models make use of a constant $\chi(g)$ [15,20]. For initial conditions $n(x,0)$ with compact support, the traveling wave solutions are monotonically decreasing and shock-fronted. Recent theoretical work has demonstrated the existence of a wide range of traveling wave solutions with complex nonmonotone shapes and multiple discontinuities [8]. These solutions are obtained by using different $\chi(g)$ functions. The intricate detail of these solutions means that they are ideal for benchmarking since several features of the solution, such as the speed of invasion, length and position of discontinuities and the location of turning points in the solution can be used for algorithm benchmarking.

3. Phase plane analysis

Introducing the traveling wave coordinate for right-moving waves, $z = x - ct$ where $c > 0$ is the dimensionless wave speed, the conservation system can be written as a system of first order odes on $-\infty < z < \infty$:

$$-c\frac{\mathrm{d}n}{\mathrm{d}z} = -\frac{\mathrm{d}}{\mathrm{d}z}\left(\chi(g)n\frac{\mathrm{d}g}{\mathrm{d}z}\right) + f, \quad -c\frac{\mathrm{d}g}{\mathrm{d}z} = h. \tag{2}$$

Combining these equations gives

$$\frac{\mathrm{d}n}{\mathrm{d}z} = \frac{F(g,n)}{W(g,n)}, \quad \frac{\mathrm{d}g}{\mathrm{d}z} = -\frac{1}{c}h(g,n), \tag{3}$$

where

$$F(g,n) = -\frac{1}{c}\left[f - nh\left(\frac{\chi'}{c^2}h + \frac{\chi}{c^2}h_g\right)\right], \quad W(g,n) = 1 + \frac{\chi}{c^2}(h + nh_n), \tag{4}$$

where $\chi' = \mathrm{d}\chi(g)/\mathrm{d}g$ and partial derivatives are denoted with subscripts.

In the (g,n) phase plane, the n-nullcline is given by $F(g,n) = 0$, provided $W(g,n) \neq 0$ simultaneously. In fact the derivative $\mathrm{d}n/\mathrm{d}z$ is undefined along the curve where $W(g,n) = 0$. This is referred to as a "wall of singularities" [16]. Trajectories approaching the wall of singularities can only pass through the wall at special points where $W(n,g) = F(n,g) = 0$. Such a point is called a "hole in the wall" [16]. At these points, $\mathrm{d}n/\mathrm{d}z$ is finite.

For our choice of kinetics f and h in (1) we seek a trajectory in the (g,n) phase plane connecting the steady states $(\beta/(\beta+\gamma),1)$ and $(1,0)$. Such solutions exist for every $c \geqslant c_{\min}$ [7]. Discontinuous solutions are permitted and the details can be derived using the Lax entropy condition and the Rankine–Hugoniot jump condition [4,10,11]. The jump condition shows that both n and $\partial g/\partial x$ can support a discontinuity while g is continuous. The value of the dependent variables on the left and right side of the jump discontinuity are denoted with subscripts L and R. The jump condition for n is $W(g,n^*) = 0$ with $n^* = (n_{\mathrm{L}} + n_{\mathrm{R}})/2$. This means that any discontinuity in n always jumps the wall of singularities with the wall located at the center of the jump. The length of the discontinuity in n will be denoted as $\Lambda = n_{\mathrm{L}} - n_{\mathrm{R}}$. For our kinetics, at the minimum wave speed $c_{\min}$, the value of n at the endpoints of the leading shock are given by $n_{\mathrm{R}} = 0$ and $n_{\mathrm{L}} = c_{\min}^2/(\gamma\chi(1))$. Therefore, the length of the leading shock is given by

$$\Lambda = \frac{c_{\min}^2}{\gamma\chi(1)}. \tag{5}$$

This quantity is used to assess algorithm performance.

The location of the wall, nullclines, steady states, and vectors defining the joining trajectory are known exactly for any given $c \geqslant c_{\min}$. The trajectories are numerically generated using standard Mathematica ode routines. The initial point used to solve for the trajectory which connects the two steady states is iteratively determined. Only the case $c = c_{\min}$ is considered here.

4. Numerical solution

We solve (1) on $0 < x < L$ where L is large enough to allow the formation of traveling waves with constant speed and shape. Zero flux boundary conditions are imposed at $x = 0$. The long term traveling waves, moving at the minimum wave speed $c_{\min}$, are independent of the initial condition provided that $n(x,0)$ has compact support. We set $n(x,0) = 1 - \mathrm{H}(x-1)$ and $g(x,0) = 1$ for all $0 < x < L$ where H is the Heaviside step function.

Numerical solutions are obtained with a high-resolution central scheme by Kurganov and Tadmor [6]. Details of the implementation are given previously [6,20]. This algorithm is chosen since it is known to perform well for similar problems involving nonlinear HCLs with discontinuous solutions [7]. Uniform spatial and temporal discretizations are chosen to give grid independent results. A minmod flux limiter is used and the temporal integration is performed with a third order Runge Kutta algorithm. At each time step the location of a particular contour $n(x,t) = \hat{n}$ is evaluated and used to approximate the wave speed c over successive time steps. Simulations are performed until c settles to a constant.

5. Results and discussion

Recent analysis has shown that a rich variety of nonmonotone invasion profiles can be generated by varying $\chi(g)$ [8]. We focus on two trigonometric forms given by

$$\chi(g) = 2 + \sin(k\pi g), \quad \chi(g) = 2 + \cos(k\pi g), \tag{6}$$

where k is a positive integer, giving $\chi(g) > 0$.

Traveling wave solutions are generated with the pde solver and the solutions compared with phase plane results, using both the sine and cosine $\chi(g)$ functions for various values of k. Detailed profiles are given for $k = 1$ and $k = 4$ for the sine function in Fig. 1. The traveling wave solutions have a discontinuous leading edge which has been translated so it is positioned at $x = 0$. These profiles demonstrate the general behaviour of the chemotaxis system and illustrate how the pde solver performs relative to the phase plane analysis. Three kinds of quantitative comparison are made. First, the (g, n) coordinate of turning points of n in the numerical profile are compared to the (g, n) coordinate in the phase plane where the solution trajectory intersects a nullcline. Second, the (g, n) coordinate of any discontinuities in the numerical profile of n are compared to the (g, n) coordinate of any jumps in n in the phase plane. Third, the length of any discontinuity in n in the numerical profile should correspond to the length of the discontinuity in n in the phase plane. We note that other than indicating the length of a discontinuity in n, the location of the wall and

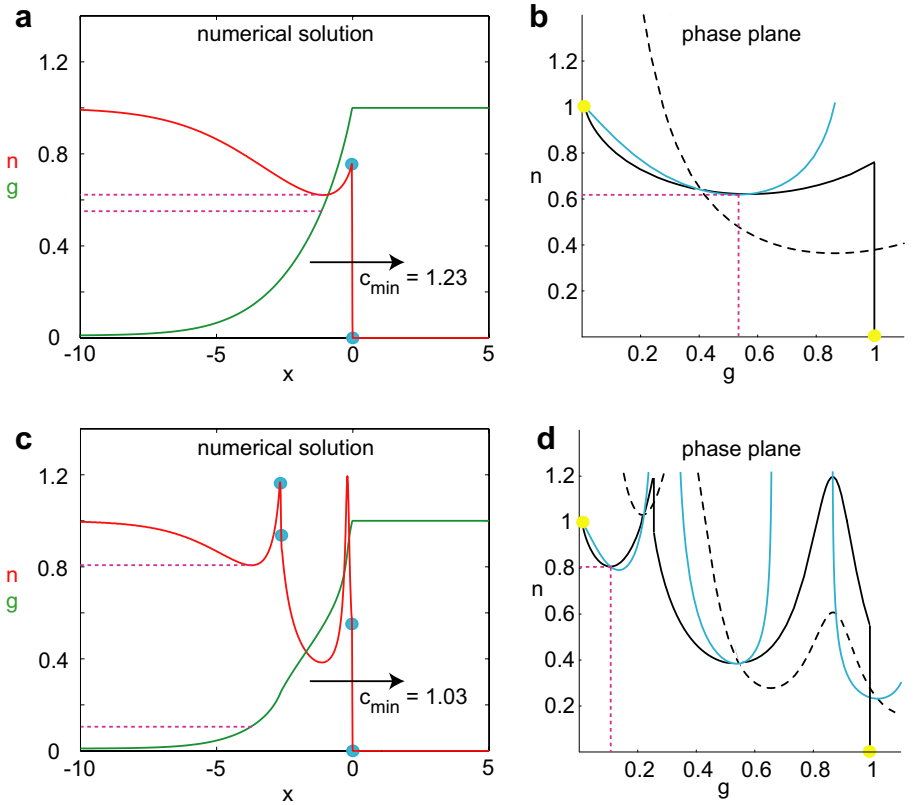

Fig. 1. Comparison of numerical and phase plane results for nonmonotone chemotactic invasion. The endpoints of the discontinuities in the pde solution are shown with a blue dot and the nondimensional invasion speed is shown. The trajectory in the phase plane is shown with a solid black line joining the two steady states shown with yellow dots. The dotted line is the wall $W(g, n) = 0$ and the nullcline is in blue $F(g, n) = 0$. Results in (a) and (b) correspond to $\chi(g) = 2 + \sin(\pi g)$. The traveling waves in (a) and (b) are oscillatory and shock-fronted. The location of the turning point in n is identified and the (g, n) coordinates are digitized (dotted magenta lines) showing that both the numerical and phase plane results give the location of the turning point as $(g, n) = (0.56, 0.62)$. Results in (c) and (d) show equivalent results for $\chi(g) = 2 + \sin(4\pi g)$. The traveling waves in (c) and (d) show a more intricate invasion profile with multiple discontinuities and several turning points. The location of the left-most turning point in n is identified and the (g, n) coordinates are digitized (dotted magenta lines) showing that both the numerical and phase plane results give the location of the turning point as $(g, n) = (0.11, 0.81)$. All results correspond to $\beta = 0.01$ and $\gamma = 1$. The pde solver used $\Delta x = 0.01$ and $\Delta t = 0.005$.

Table 1
Summary of nonmonotone invasion profiles showing details of the wavespeed, position and coordinates of the turning points and discontinuities

$\chi(g)$	Speed $c_{\min}$	Turning point 1 (x,g,n)	Turning point 2 (x,g,n)	Turning point 3 (x,g,n)	Discontinuity 1 (x,g,n_L,n_R)	Leading shock length Λ	Discontinuity 2 (x,g,n_L,n_R)
$2+\sin(\pi g)$	1.23	(−1.1,0.56,0.62)	–	–	(0,1,0.76,0)	0.76	–
$2+\sin(2\pi g)$	0.93	(−1.6,0.28,0.65)	(−0.5,0.71,1.12)	–	(0,1,0.43,0)	0.43	–
$2+\sin(3\pi g)$	1.14	(−3.7,0.15,0.79)	(−0.9,0.72,0.37)	–	(0,1,0.65,0)	0.65	(−2.5,0.37,1.27,0.79)
$2+\sin(4\pi g)$	1.03	(−3.7,0.11,0.81)	(−1.1,0.54,0.38)	(−0.2,1.19,0.86)	(0,1,0.53,0)	0.53	(−2.6,0.25,1.17,0.94)
$2+\cos(\pi g)$	0.93	(−1.5,0.31,0.70)	(−0.1,0.90,0.90)	–	(0,1,0.86,0)	0.86	–
$2+\cos(2\pi g)$	1.05	(−3.8,0.11,0.84)	(−2.7,0.28,0.97)	(−0.4,0.35,0.88)	(0,1,0.37,0)	0.37	–
$2+\cos(4\pi g)$	1.04	(−1.5,0.42,0.46)	(−0.6,0.74,1.35)	–	(0,1,0.36,0)	0.36	–

All solutions correspond to $\beta = 0.01$, $\gamma = 1$ and $c = c_{\min}$. All (g,n) coordinates from both the numerical and phase plane results correspond identically. The leading shock length Λ corresponds to the length of discontinuity 1 given in column 6.

holes in the phase plane do not correspond to any properties of the numerical solution that are discernable or comparable.

Results for the sine $\chi(g)$ with $k = 1$ in Fig. 1a and b show an oscillatory invasion profile with one turning point in n and a discontinuous front. The numerical and analytical coordinates of the turning points can be quantitatively compared. For example, the location of the turning point in Fig. 1a is digitized from the numerical profile to give $(g,n) = (0.56, 0.62)$. In the phase plane, the solution trajectory intersects the nullcline at the same value of (g,n). Therefore, we observe an exact correspondence between the numerical simulation and analysis. The endpoints of the discontinuity in n are clearly shown in Fig. 1a and b. The length of the leading shock predicted numerically can be determined by digitizing the height of the discontinuity at $x = 0$ in Fig. 1a giving $\Lambda = 0.76$. This result is corresponds exactly with the phase plane analysis through Eq. (5). Hence, the numerical results coincide with the analysis giving confidence in the numerical solution.

Results for the sine $\chi(g)$ with $k = 4$ are given in Fig. 1c and d showing a stunningly complex invasion profile with two discontinuities and three turning points in n. The coordinates of these features were quantitatively checked with the corresponding points in the phase plane. This comparison shows again that the pde solver accurately captures the details of this fascinating invasion profile.

Detailed results are summarized in Table 1 showing (i) the invasion speed $c_{\min}$, (ii) the coordinates of turning points in n, and (iii) the coordinates and length of discontinuities in n. This table contains data that has been generated by digitizing results from both the numerical profiles and phase plane trajectories as well as using Eq. (5) to predict the length of the leading shock. In all cases we found that the results from the phase plane are identically replicated by the numerical algorithm within two decimal places. This data is suitable for algorithm benchmarking purposes. Each of these seven traveling wave profiles are characterized by having an oscillatory region just behind the leading shock. Results for the cosine $\chi(g)$ function with $k = 3$ are not included in the table. In this case the invasion profile contains a turning point that is very close behind the leading shock. It is difficult to digitize these details from the numerical solution. This case should not be used for algorithm benchmarking.

6. Conclusion

The chemotaxis invasion problem described here constitutes a challenging numerical test case for HCL algorithm development. The invasion problem involves nonlinearities and coupling in both the flux and source terms of the hyperbolic system. This test case is more challenging than other standard HCL test cases with the advantage of being analytically tractable. Data corresponding to particular invasion shapes are presented for benchmarking purposes.

Most previously documented shock-fronted chemotactic traveling wave profiles have been limited to constant $\chi(g)$. These profiles have simple shapes and are therefore not particularly well-suited for algorithm benchmarking. Recent analysis has demonstrated the existence of nonmonotone traveling wave invasion

profiles with multiple discontinuities. Such profiles are obtained by choosing different $\chi(g)$ functions. These nonmonotone invasion profiles are ideal for algorithm testing as the details of the invasion profiles, such as the position of turning points and discontinuities, can be deduced in the phase plane and used to assess algorithm performance.

It is interesting to remark that the use of HCLs with solutions containing oscillations behind a shock for algorithm testing is unique. A key requirement of numerical algorithms for HCLs is the preclusion of artificial numerical oscillations. Given that most invasion profiles reported in the literature have monotonically decreasing shapes coupled with the historical prevalence of artificial oscillations associated with numerical solutions of HCLs, it is possible that the invasion profiles presented here might, at first glance, appear to be affected by numerical error. The phase plane analysis shows that the nonmonotone invasion profiles are expected and ought to be replicated by a numerical algorithm. Therefore we suggest that in addition to testing an algorithm's ability to accurately simulate monotone solutions, an algorithm should also be able to accurately simulate problems with true oscillations and shocks. The chemotactic invasion profiles described here, with an oscillatory region behind the leading shock, provide such test cases and are therefore naturally of interest to algorithm developers within the computational fluid dynamics community.

Acknowledgement

This work is supported by the National Health and Medical Research Council and the Australian Research Council (ARC). Mat Simpson is an ARC Postdoctoral Fellow. Kerry Landman is supported by the Particulate Fluids Processing Centre, an ARC Special Research Centre. We thank the two anonymous reviewers for their comments.

References

[1] O.R. Burggraf, Analytical and numerical studies of the structure of steady separated flows, J. Fluid Mech. 24 (1966) 113–151.
[2] M.A. Christon, D.I. Ketcheson, A.C. Robinson, An assessment of semi-discrete central schemes for hyperbolic conservation laws, SANDIA National Laboratories Report. SAND2003-3238, 2003.
[3] J. Donea, A. Huerta, Finite Element Methods for Flow Problems, John Wiley and Sons, West Sussex, England, 2003.
[4] R. Courant, D. Hilbert, Methods of Mathematical Physics, 2nd ed., vol. 2, Interscience, New York, 1964.
[5] H.R. Henry, Effects of dispersion on salt encroachment in coastal aquifers. In Sea Water in Coastal Aquifers, US Geological Survey Supply Paper 1613-C: 70-84, 1964.
[6] A. Kurganov, E. Tadmor, New high-resolution central schemes for nonlinear conservation laws and convection–diffusion equations, J. Comp. Phys. 160 (2000) 241–282.
[7] K.A. Landman, M.J. Simpson, J.L. Slater, D.F. Newgreen, Diffusive and chemotactic cellular migration: Smooth and discontinuous travelling wave solutions, SIAM J. Appl. Math. 65 (2005) 1420–1442.
[8] K.A. Landman, M.J. Simpson, G.J. Pettet, Nonmonotonic tactic travelling waves. Submitted for publication.
[9] M. Le Bars, M. Grae Worster, Solidification of a binary alloy: Finite-element single-domain simulation and new benchmark solutions, J. Comp. Phys. 216 (2006) 247–263.
[10] R.J. LeVeque, Finite volume methods for hyperbolic problems, Cambridge University Press, Cambridge, United Kingdom, 2002.
[11] R.C. McOwen, Partial Differential Equations, 3rd ed., Prentice Hall, NJ, 1996.
[12] W.L. Oberkampf, T.F. Trucano, Verification and validation in computational fluid dynamics, Prog. Aerosp. Sci. 38 (2002) 209–272.
[13] N. Oreskes, K. Shrader-Frechette, K. Belitz, Verification, validation and confirmation of numerical models in the earth sciences, Science 263 (1994) 641–646.
[14] M. Pelanti, R.J. LeVeque, High-resolution finite volume methods for dusty gas jets and plumes, SIAM J. Sci. Comput. 28 (2006) 1335–1360.
[15] A.J. Perumpanani, J.A. Sherratt, J. Norbury, H.M. Byrne, A two parameter family of travelling waves with a singular barrier from the modelling of extracellular matrix mediated cellular invasion, Physica D 126 (1999) 145–159.
[16] G.J. Pettet, D.L.S. McElwain, J. Norbury, Lotka–Volterra equations with chemotaxis: Walls barriers and chemotaxis, IMA J. Math. Appl. Med. 17 (2000) 395–413.
[17] D.J. Price, J.J. Monaghan, Smoothed particle magnetohydrodynamics – I: Algorithm tests in one dimension, Mon. Not. R Astron. Soc. 348 (2004) 123–138.
[18] C.T. Simmons, K.A. Narayan, R.A. Wooding, On a test case for density dependent groundwater flow and solute transport models: the salt lake problem, Water Resour. Res. 35 (1999) 3607–3620.

[19] M.J. Simpson, T.P. Clement, Improving the worthiness of the Henry problem as a benchmark for density-dependent groundwater flow models, Water Resour. Res. 40 (2004) W01504, doi:10.1029/2003WR002199.
[20] M.J. Simpson, K.A. Landman, D.F. Newgreen, Chemotactic and diffusive migration on a non-uniformly growing domain: Numerical algorithm development and applications, J. Comput. Appl. Math. 192 (2006) 282–300.
[21] G.A. Sod, A survey of several finite difference methods for systems of nonlinear hyperbolic conservation laws, J. Comp. Phys. 27 (1978) 1–31.
[22] R.A. Wooding, Growth of fingers at an unstable diffusing interface in a porous medium or Hele-Shaw cell, J. Fluid Mech. 39 (1969) 195–477.
[23] X. Ying, A.A. Khan, S.S.Y. Wang, Upwind conservative scheme for the Saint Venant equations, J. Hydraul. Eng. – ASCE 130 (2004) 977–987.